A first search for argon-bound neutron-antineutron oscillation using the MicroBooNE LArTPC

The MicroBooNE Collaboration

MICROBOONE-NOTE-1113-PUB
microboone_info@fnal.gov

Abstract

The use of Liquid Argon Time Projection Chambers (LArTPCs) as a detector technology in neutrino experiments has grown considerably over the past two decades. The excellent spatial and calorimetric resolution offered by LArTPCs enable precise neutrino oscillation measurements as well as beyond-Standard Model searches. One such search, which is the focus of this note, is the search for nucleus-bound neutron-antineutron ($n - \bar{n}$) oscillation. The $n - \bar{n}$ oscillation process is a baryon number violating process that produces a unique, star-like topology as a result of multiple final state pions. This unique signature is a key feature that may be used to search for this signal process. This note describes a machine learning-based analysis of MicroBooNE data, making use of a sparse convolutional neural network to search for $n - \bar{n}$ oscillation-like signals in MicroBooNE. While the future DUNE LArTPC can search for this signature with high sensitivity, existing MicroBooNE data can be used to demonstrate and validate methodologies that can be used as part of the DUNE search. This document presents the first-ever search for $n - \bar{n}$ oscillation in a LArTPC, using MicroBooNE off-beam data (data collected when the neutrino beam was not running).

Contents

1 Introduction

A nucleus-bound neutron-antineutron ($n-\bar{n}$) oscillation is a process where a neutron spontaneously transforms into an antineutron. The resulting antineutron annihilates with a neighboring nucleon (proton or neutron) producing, on average, 3-4 final state pions, with zero net momentum and a total energy corresponding to approximately the sum of the mass of the two nucleons. This energetic interaction creates a star-like topology, a striking signature to search for this signal process and separate it from background processes.

$n-\bar{n}$ oscillation is a theoretically motivated beyond-Standard Model process that violates baryon number by two units [1] [2]. A discovery or stringent lower bound on its transition rate would make an important contribution to our understanding of the baryon asymmetry in the Universe. To date, limits are provided on the lifetimes of this process by various experiments using either free neutrons or bound neutrons in nuclei [3–12] The most stringent limit on the lifetime of this process is provided by the Super-Kamiokande experiment [13].

There is an opportunity to perform a high sensitivity search with the future Liquid Argon Time Projection Chamber (LArTPC)-based DUNE detector [14]. This note discusses the methodology for the $n-\bar{n}$ oscillation search using the MicroBooNE detector [15] which also employs LArTPC technology. The objective of the $n-\bar{n}$ search in MicroBooNE is not to set a competitive $n-\bar{n}$ lifetime limit, but to serve as first ever demonstration of an $n-\bar{n}$ search in a liquid argon detector and as a testbed for the future DUNE experiment. It is worth mentioning that the key difference between the search strategy of MicroBooNE and DUNE would be related to the nature of background. In MicroBooNE, a surface detector, the dominant background for the $n-\bar{n}$ signal process is cosmogenic background (predominantly cosmic ray muons and/or products of their electromagnetic and hadronic showers), whereas for DUNE the dominant background is expected to be from high-energy atmospheric neutrinos interacting in the detector through neutral current interactions.

2 Analysis Overview

The analysis begins by simulating the signal ($n-\bar{n}$) and background samples. A data driven approach is used to simulate the cosmogenic background which enables accurate modeling of cosmogenics and noise sources, including any time-dependence. Furthermore, the first iteration of this analysis used CORSIKA simulated background which leads to discrepancy in data and Monte Carlo (MC) [16]. To overcome these data-MC differences, MicroBooNE's off-beam data, collected using triggers outside the beam window, are used. The signal samples are generated overlaying the signal $n-\bar{n}$ events on the top of off-beam data as shown in Fig. 1. To simulate $n-\bar{n}$ events uniformly across the detector's active volume (85 tonnes), MicroBooNE uses the GENIE neutrino event generator (GENIE v.3.00.04) [17] to model the initial state nucleon Fermi momentum, binding energy, and final state interactions. The simulated interaction is subsequently processed with Geant4 [18] and detector simulation. These simulation stages (GENIE, Geant4, and detector simulations) can also alter the appearance of the signal event and therefore will be considered as systematic sources of uncertainty.

A single signal $n-\bar{n}$ interaction is simulated in each event (also referred to as an "exposure interval", consisting of a 2.3ms time interval). The events include multiple reconstructed particle interactions in the liquid argon volume; they are called "clusters" (3D objects which are collections of spacepoints as a result of the Wire-Cell cluster reconstruction where each spacepoint carries information about the wire position, time-tick, and charge deposition) [19]. Following cluster

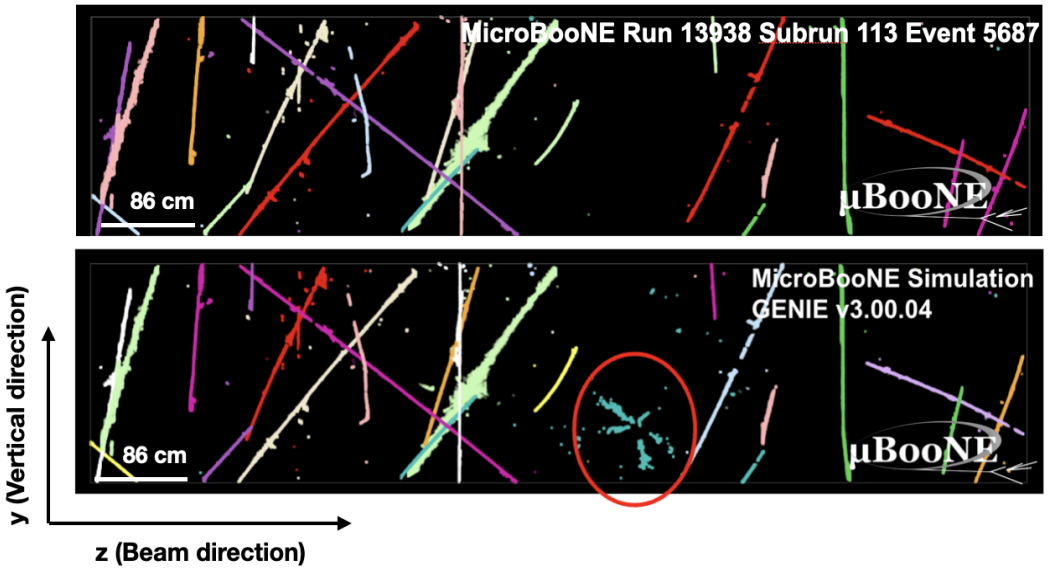

Figure 1: *(top) Event display showing background sample. (bottom) Event display showing an $n-\bar{n}$ signal sample (highlighted in red circle) overlaid on the top of background sample. The x-axis represents z direction (beam direction) and y-axis is the vertical direction. The view in this image is front view (YZ) of the detector. Color represents charge deposition. For the background sample, MicroBooNE off-beam data is used. For the signal simulation, a GENIE-simulated interaction is overlaid on MicroBooNE off-beam data.*

reconstruction, a preselection using a multi-variate algorithm Boosted Decision Tree (BDT) is developed. The preselection aims to significantly reduce the background rate (predominantly cosmic ray muons) while maintaining high signal efficiency. The BDT is trained using variables that contain information about position and time associated with the spacepoints. Details about the BDT are given in Appendix A. The training outcome is shown in Fig. 2 (left) where a clear separation is seen between the signal ($n-\bar{n}$) and background (cosmic) processes. By selecting clusters with BDT>0.1, the $n-\bar{n}$ cluster selection efficiency (86.48%) is about 10 times higher than the cosmic cluster selection efficiency (8.58%).

These clusters are further used for developing the final selection based on image analysis using a sparse Convolution Neural Network (CNN) [20] [21]. The performance of sparse CNN has previously been validated using MicroBooNE data [22] [23]. For this analysis, the 2D projections on MicroBooNE's three planes, because of their resemblance with 2D pixeled RGB images, are used as the CNN input. These 2D projections are formatted in such a way as to retain only the important pixels. The wire position, time-tick, and charge deposition is saved only for those spacepoints associated with signal or background clusters. This way of saving the localized clusters rather than the entire readout image is highly memory-efficient. Further details on the CNN are provided in Appendix B.

The CNN training results are shown in Fig. 2 (middle). The CNN score cut for the final selection is optimized with respect to the projected sensitivity using a statistically independent sample with sufficient statistics (nearly 1.6M events). As a prerequisite for the sensitivity calculation, the background is estimated and efficiencies for signal and background events are evaluated by varying CNN score cuts which are represented by orange stars in Fig. 2 (right) and are shown in Tab. 1. The statistical uncertainty on the background estimate as well as on signal and background efficiencies are shown in Tab. 1. For these particular selection efficiencies, preliminary sensitivity values are calculated, using the TRolke package in ROOT [24], by assuming a conservative estimate of 15% systematic uncertainty. These are shown in Tab. 1. Considering sensitivity as a figure of

merit, the optimal CNN cut is found to be 0.800, achieving 73.6±0.034 % signal efficiency and $8.77\times10^{-3}\pm7.4\times10^{-4}$ % background efficiency.

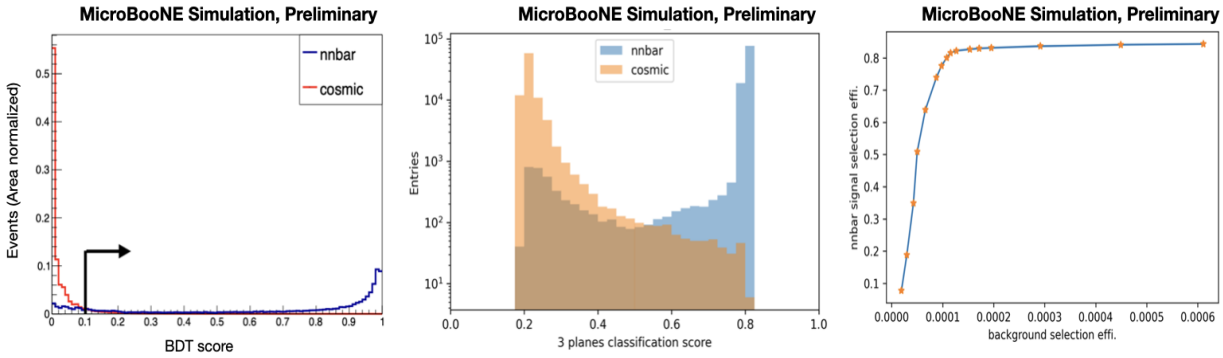

Figure 2: *(left) Classification performance of the BDT for the $n-\bar{n}$ and cosmic clusters. The entries are area-normalized. (middle) CNN score distribution for the $n-\bar{n}$ and cosmic clusters. (right) Signal selection efficiency versus background selection efficiency after final selection, varying the CNN score cut, where the cut values are [0.77, 0.78, 0.79, 0.795, 0.796, 0.797, 0.798, 0.7985, 0.799, 0.7995, 0.800, 0.801, 0.802, 0.803, 0.804, 0.805] represented by orange stars*

CNN cut	Signal effi.	Bkg. effi.	Bkg. estimate	Sensitivity
0.797	0.827 ± 0.0003	1.53e-4 ± 9.7e-6	24.8 ± 1.6	2.62e+25 yrs
0.798	0.822 ± 0.0003	1.27e-4 ± 8.8e-6	20.5 ± 1.4	2.83e+25 yrs
0.799	0.801 ± 0.00031	1.08e-4 ± 8.2e-6	17.5 ± 1.3	2.98e+25 yrs
0.800	0.736 ± 0.00034	8.77e-5 ± 7.4e-6	14.2 ± 1.2	2.99e+25 yrs
0.801	0.639 ± 0.00038	6.61e-5 ± 6.4e-6	10.7 ± 1.0	2.95e+25 yrs
0.802	0.508 ± 0.00039	5.0e-5 ± 5.6e-6	8.1 ± 0.9	2.65e+25 yrs
0.803	0.349 ± 0.00037	4.26e-5 ± 5.1e-6	6.9 ± 0.8	1.95e+25 yrs

Table 1: *Preliminary sensitivity around the optimized CNN cut 0.800. The signal and background efficiencies and the background estimate are shown. The errors shown indicate finite-MC statistical uncertainties.*

Table 2 shows the number of entities for each reconstruction and selection stage. During the preselection, the number of cosmic clusters is reduced, and the number of $n-\bar{n}$ clusters and cosmic clusters per event become of the same order. Then, the number of cosmic clusters is highly suppressed after the final selection, while the number of $n-\bar{n}$ clusters remains high.

3 Sensitivity Calculation

The sensitivity for MicroBooNE's $n-\bar{n}$ search is calculated assuming 372 seconds of exposure (equal to the data exposure that will be used to make this measurement in the future), corresponding to 3.13 neutron·years and considering statistical uncertainties only. This is shown in Tab. 3. The Rolke method uses a frequentist approach to evaluate the sensitivity and limits. There are various models within the TRolke package to account for signal selection efficiency and background contamination. This analysis uses a Gaussian model, which considers Gaussian

Entities	$n-\bar{n}$	cosmic
Events	1,633,525	1,618,827
Reconstructed clusters	1,684,516	14,857,224
Clusters (after pre-selection)	1,455,214	1,283,074
Clusters (after final-selection)	1,207,153	142
Events (after final-selection)	1,202,281	142
Selection efficiency	0.736	8.77e-5

Table 2: *The number of entities for each reconstruction and selection stage. The numbers are evaluated using a factor of 10 larger exposure than will be used for the data analysis. The selection efficiency indicates the ratio between the 'Events' and 'Events (after final-selection)'.*

background and signal efficiency that includes the expectation along with a standard deviation for both the background and selection efficiency. A similar procedure was used by SNO [12] and Super-K [13]. Table 3 provides the sensitivity using 372 seconds of exposure and accounting for statistical uncertainty only.

Uncertainty assumed on signal and backgrounds	Sensitivity (Rolke)
Finite MC Stat.	3.09 e+25 years

Table 3: *90% C.L. sensitivity for the $n-\bar{n}$ oscillation lifetime assuming a 372 second exposure in MicroBooNE considering only statistical uncertainties.*

4 Conclusion

This note presents the methodology for the first-ever search for argon-bound neutron-antineutron oscillation, using a 372-second exposure in the MicroBooNE LArTPC. The analysis and selection makes use of state-of-the-art reconstruction tools, including deep learning methods developed for LArTPC experiments, and has a signal efficiency of 73.6%. The sensitivity for the $n-\bar{n}$ search is calculated considering only statistical uncertainties. The analysis is ongoing. The effects of various systematic uncertainties and validation with fake-data sample is being evaluated.
Although the $n-\bar{n}$ search in MicroBooNE is not aimed to provide competitive limits, this analysis serves as a demonstration for the capability of future larger and well-shielded LArTPC's, including the future experiment DUNE, to perform such searches for baryon number violation with high sensitivity.

References

[1] K. S. Babu, P. S. Bhupal Dev, E. C. F. S. Fortes, and R. N. Mohapatra, "Post-Sphaleron Baryogenesis and an Upper Limit on the Neutron-Antineutron Oscillation Time," *Phys. Rev. D 87, 115019.*

[2] J. M. Arnold, B. Fornal, and M. B. Wise, "Simplified models with baryon number violation but no proton decay," *Phys. Rev. D 87, 075004.*

[3] M. L. Cherry, K. Lande, C. K. Lee, R. I. Steinberg, and B. Cleveland, "Experimental test of baryon conservation: A new limit on neutron-antineutron oscillations in oxygen," *Phys. Rev. Lett. 50, 1354.*

[4] T. W. Jones *et al.* (Irvine-Michigan-Brookhaven Collaboration), "Search for $n - \bar{n}$ oscillation in oxygen," *Phys. Rev. Lett. 52, 720.*

[5] G. Fidecaro *et al.* (CERN-ILL-Padova-Rutherford-Sussex Collaboration), "Experimental search for neutron anti-neutron transitions with free neutrons," *Phys. Lett. B 156, 122.*

[6] M. Takita *et al.* (Kamiokande Collaboration), "Search for neutron-antineutron oscillation in ^{16}O nuclei," *Phys. Rev. D 34, 902.*

[7] G. Bressi *et al.* , "Final results of a search for free neutron anti-neutron oscillations," *Nuovo Cim. A*, vol. 103, pp. 731–750, 1990.

[8] Ch. Berger *et al.* (Frejus Collaboration), "Search for neutron-antineutron oscillations in the Frèjus detector," *Phy. Lett. B*, vol. 240, no. 1, pp. 237–242, 1990.

[9] K. Abe *et al.* (Super-Kamiokande Collaboration), "Search for $n - \overline{n}$ oscillation in super-kamiokande," *Phys. Rev. D 91, 072006.*

[10] M. Baldo-Ceolin *et al.*, "A new experimental limit on neutron-antineutron oscillations," *Zeitschrift für Physik C Particles and Fields*, vol. 63, no. 3, pp. 409–416, 1994.

[11] J. Chung *et al.*, "Search for neutron-antineutron oscillations using multiprong events in soudan 2," *Phys. Rev. D 66, 03204.*

[12] B. Aharmim *et al.* (SNO Collaboration), "Search for neutron-antineutron oscillations at the sudbury neutrino observatory," *Phys. Rev. D 96, 092005.*

[13] K. Abe *et al.* (Super-Kamiokande Collaboration), "Neutron-antineutron oscillation search using a 0.37 megaton-years exposure of super-kamiokande," *Phys. Rev. D 103, 012008.*

[14] B. Abi *et al.* (DUNE Collaboration), "Prospects for beyond the standard model physics searches at the deep underground neutrino experiment," *Eur. Phys. J. C (2021) 81: 322.*

[15] R. Acciarri *et al.* (MicroBooNE Collaboration), "Design and construction of the MicroBooNE detector," *Journal of Instrumentation*, vol. 12, pp. P02017–P02017, Feb 2017.

[16] P. A. *et al.* (MicroBooNE Collaboration), "Progress toward the first search for bound neutron oscillation into antineutron in a liquid argon tpc," *MICROBOONE-NOTE-1093-PUB.*

[17] J. E. Hewes, *Searches for Bound Neutron-Antineutron Oscillation in Liquid Argon Time Projection Chambers.* PhD thesis, Manchester U., 2017.

[18] D. H. Wright and M. H. Kelsey, "The Geant4 Bertini Cascade," *Nucl. Instrum. Meth. A*, vol. 804, pp. 175–188, 2015.

[19] P. Abratenko *et al.* (MicroBooNE Collaboration), "Neutrino event selection in the microboone liquid argon time projection chamber using wire-cell 3-d imaging, clustering, and charge-light matching," *JINST 16, P06043*, 2021.

[20] B. Graham, M. Engelcke, and L. van der Maaten, "3d semantic segmentation with submanifold sparse convolutional networks," *CoRR*, vol. abs/1711.10275, 2017.

[21] B. Graham and L. van der Maaten, "Submanifold sparse convolutional networks," *CoRR*, vol. abs/1706.01307, 2017.

[22] P. A. *et al.* (MicroBooNE Collaboration)", "Semantic segmentation with a sparse convolutional neural network for event reconstruction in MicroBooNE," *Phys. Rev. D 103, 052012.*

[23] P. A. *et al.* (MicroBooNE Collaboration)", "Cosmic ray muon clustering for the MicroBooNE liquid argon time projection chamber using sMask-RCNN," *arXiv:2201.05705 [hep-ex].*

[24] W. A. Rolke and A. M. López, "Confidence intervals and upper bounds for small signals in the presence of background noise," *Nucl. Instrum. Meth. A: Accelerators, Spectrometers, Detectors and Associated Equipment*, vol. 458, p. 745–758, Feb 2001.

Appendices

A - Boosted Decision Tree

A preselection using a Boosted Decision Tree (BDT) is developed making use of topological information only. The preselection aims to remove obvious cosmic clusters efficiently, thus forcing the image based final selection to learn more intricate features of more obscure backgrounds vs signal. The input variables for the BDT include topological information of the Wire-Cell reconstructed clusters, such as the number of spacepoints associated with the cluster, and the extent of the signature of the reconstructed interaction along the read-out channels (for the U, V, and Y planes) and timing information. Figure 3 shows the distributions of the following five variables for $n - \bar{n}$ (blue) and cosmic (red) clusters.

- Spacepoints: the number of cells (i.e. spacepoints) in the cluster
- Time-tick extent: (max time slice value - min time slice value) in the cluster
- Y-plane extent: (max Y-plane channel - min Y-plane channel) in the cluster
- U-plane extent: (max U-plane channel - min U-plane channel) in the cluster
- V-plane extent: (max V-plane channel - min V-plane channel) in the cluster

The XGBoost framework [**?**] is used for BDT training, for 300 iterations. The training is done using a statistically independent sample with sufficient statistics. Table 4 shows the selection efficiency for $n - \bar{n}$ and cosmic clusters with different BDT score cuts. Clusters with BDT score > 0.1 are chosen for developing the final selection. It is worth mentioning that the cut is not optimized based on any metric but is chosen to remove obvious cosmic backgrounds and retain enough background for the next selection stage of image based analysis.

	$n - \bar{n}$	cosmic	$\frac{n-\bar{n}}{\sqrt{(n-\bar{n}+cosmic)}}$
Nocut	26,525	237062	
0.05	24,400 (91.99%)	41,965 (17.7%)	94.7
0.1	22,938 (86.48%)	20,342 (8.58%)	110.3
0.15	21,867 (82.44%)	11,901 (5.02%)	119.0
0.2	21,033 (79.30%)	7,707 (3.25%)	124.1
0.25	20,551 (77.48%)	5,903 (2.49%)	126.4

Table 4: *Selection efficiency for $n - \bar{n}$ clusters and cosmic clusters obtained by varying the BDT cut. The BDT cut is chosen at 0.1, where the $n - \bar{n}$ cluster efficiency is about 10 times higher than cosmic cluster efficiency.*

Signal $n - \bar{n}$ clusters with different BDT scores are shown as 2D projections in Fig. 4. The left-hand-side figure shows the projections of an $n - \bar{n}$ cluster with a high BDT score (0.94). The right-hand-side figure shows the projections of an $n - \bar{n}$ cluster with a low BDT score (0.00145). The topology-driven pre-selection BDT, since it does not take into account the charge deposition associated with the spacepoint, can not differentiate a cosmic muon from such a straight line signal topology. However, as we expect typically more than 2 daughter particles in the pair-annihilation, such a topology is not frequent in the $n - \bar{n}$ clusters.

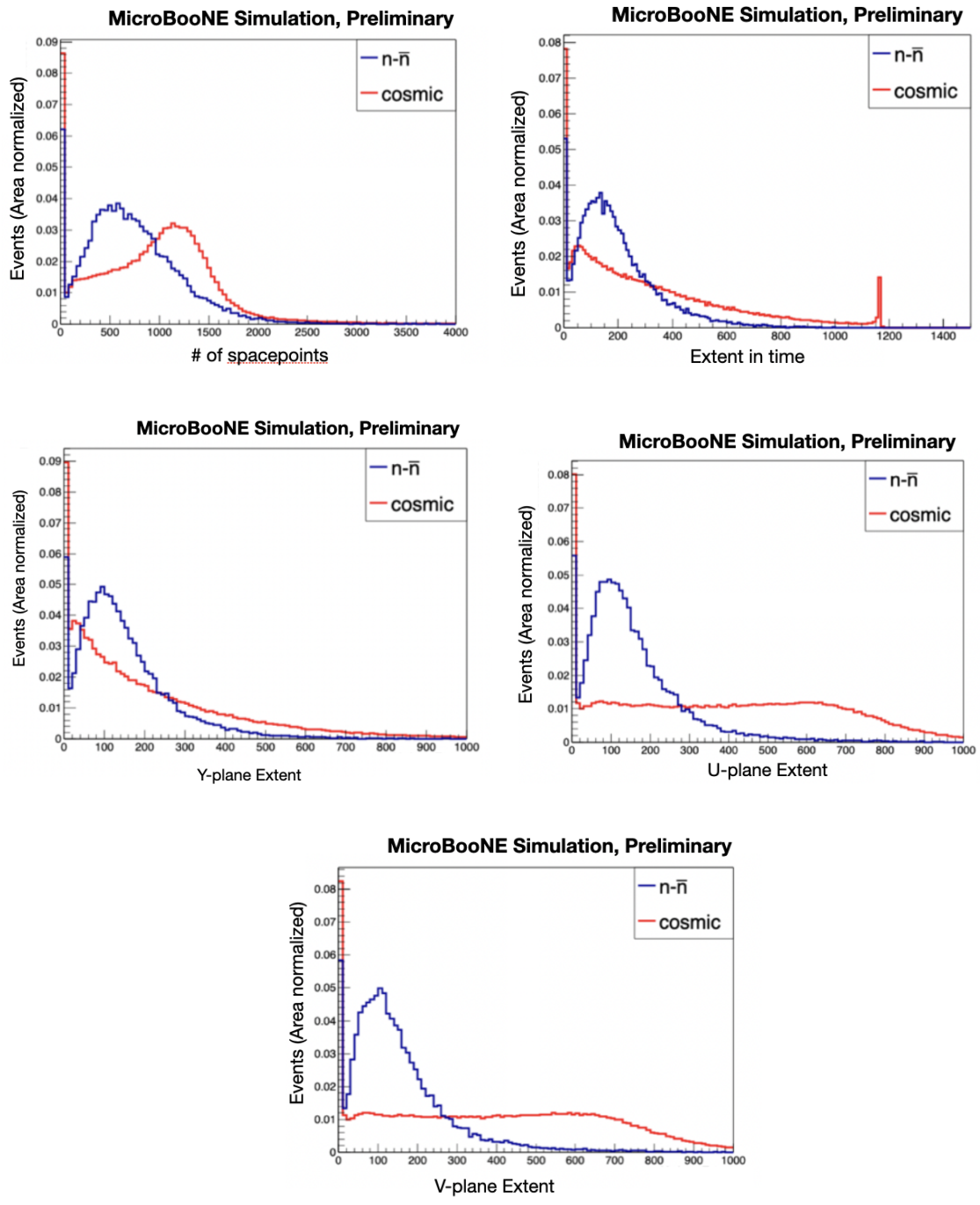

Figure 3: *Distributions for topological variables from 2D cluster projections for $n-\bar{n}$ and cosmic clusters. These variables are used for the BDT pre-selection.*

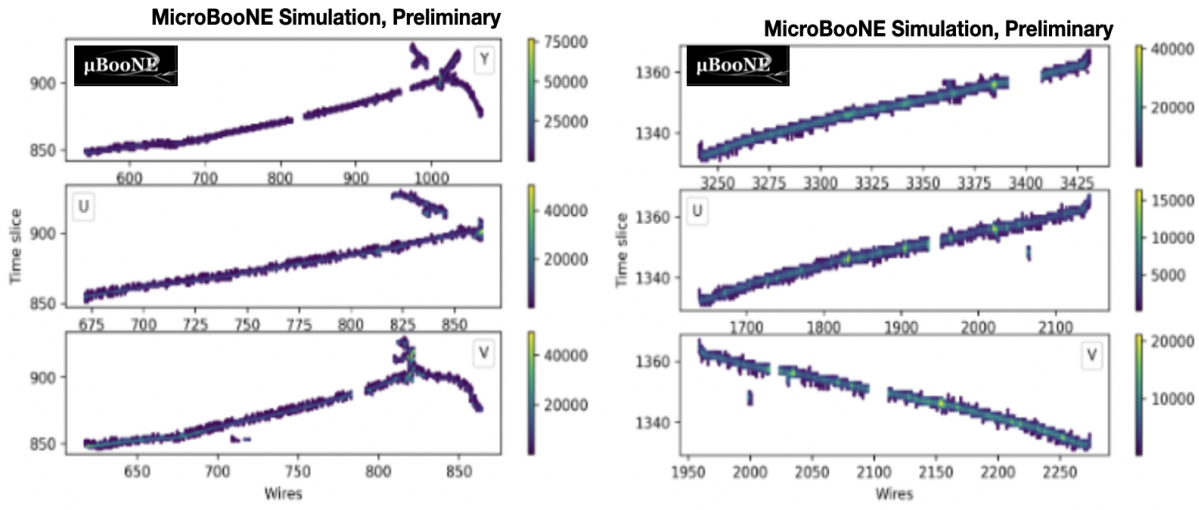

Figure 4: *(left) $n-\bar{n}$ cluster passing the BDT pre-selection with BDT score 0.94. (right) $n-\bar{n}$ cluster failing the BDT pre-selection with BDT score 0.00145.*

B - Convolution Neural Network

A sparse CNN-based classification is used to develop the final selection of this analysis using the preselected $n-\bar{n}$ and cosmic clusters. The 2D projections of the clusters, as shown in Fig. 5, on MicroBooNE's three planes (U, V, Y) are used as the CNN input. The CNN is trained and tested using statistically independent samples. The training quality is monitored using two metrics: training loss and accuracy. The training loss is a summation of the errors made for each iteration during training: the lower the loss, the better a model. However, the accuracy is determined on the final BDT iteration. Figure 6 shows the training loss (left) and accuracy (right) over 20000 iterations.

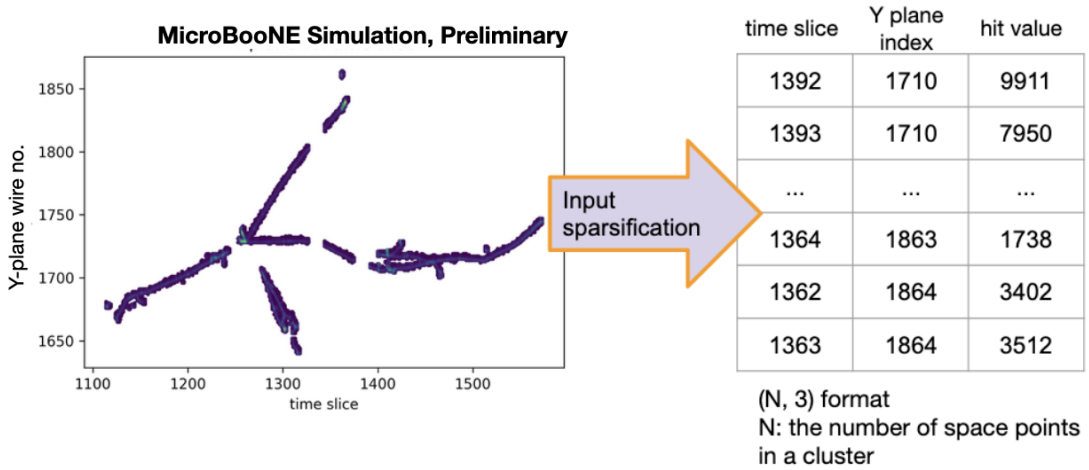

Figure 5: *(left) 2D projection of signal cluster on conventional representation. (right) The same cluster using sparsified columnar representation.*

Section 2 shows the CNN training results and optimization of the final CNN selection cut. In this section, 2D projections of some clusters passing the final selection (CNN>0.800) are shown for well-classified cases and otherwise. Figure 7 shows the 2D projections of $n-\bar{n}$ clusters passing

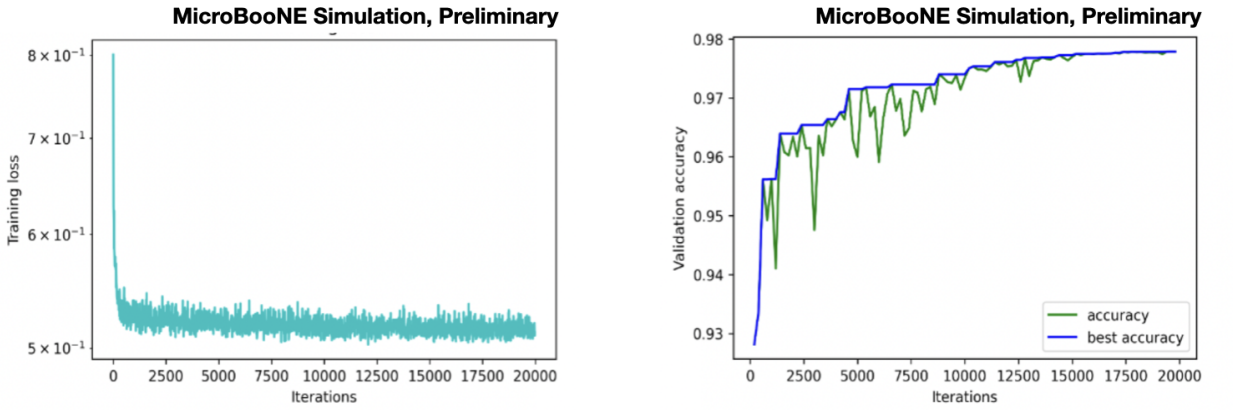

Figure 6: *(left)Monitored training loss over iterations. (right)Monitored validation accuracy over iterations. The current accuracy is shown as green solid line, the best accuracy is shown as blue solid line.*

the final selection with high CNN score. Notice the U plane projection of the left-hand-side cluster is very small, and thus looks discrete due to binning. The Y-plane, and V-plane projections show the more familiar signal topology; thus, this event scores highly on CNN classification when all planes are considered. The right-hand-side cluster demonstrates the inefficacy of U plane and V plane wires. However, the cluster is still highly scored on the CNN classification.

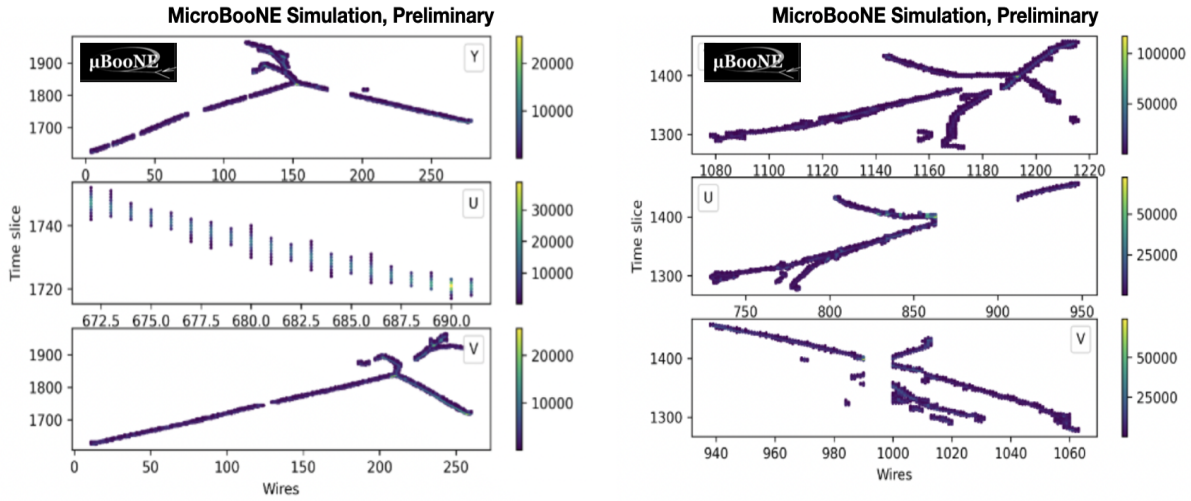

Figure 7: *(left) $n - \bar{n}$ cluster passing the BDT pre-selection with BDT score 0.981 and passing CNN selection with CNN score 0.8036. (right) $n - \bar{n}$ cluster passing the BDT pre-selection with BDT score 0.947 and passing the CNN selection with CNN score 0.804.*

Some signal clusters failed to pass the final selection as shown in Fig. 8. The left-hand-side cluster shows no reconstructed space-points on the Y-plane, and insignificant reconstruction on the U-plane. Both U-plane and V-plane signatures are small in time and wire axes. The right-hand-side cluster shows small extents on both axes as well. These clusters do not display the signature "star-like" topology and are classified with a low CNN score.

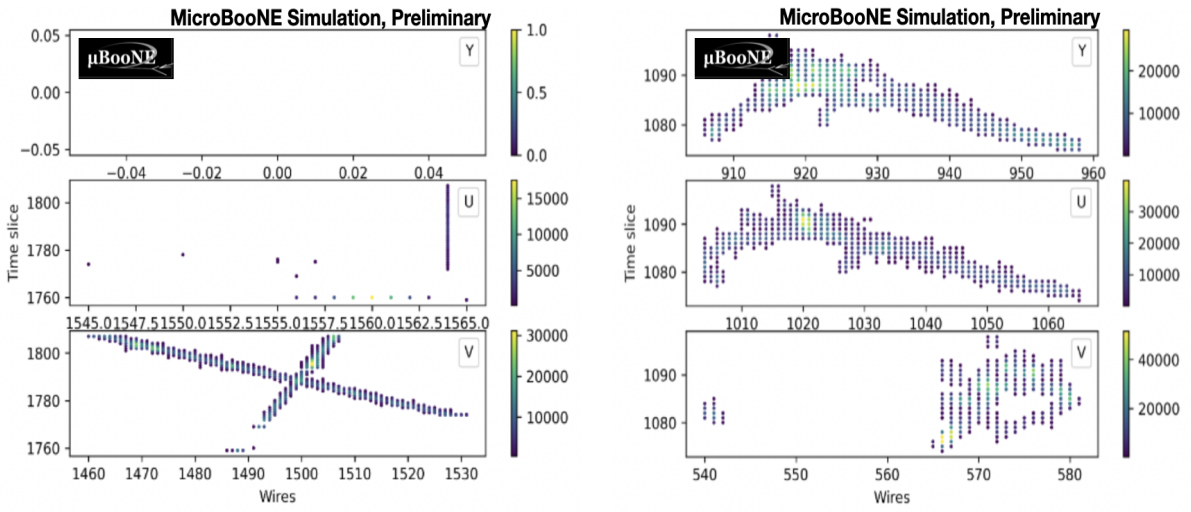

Figure 8: *(left) $n - \bar{n}$ cluster passing the BDT pre-selection with BDT score 0.177 and failing CNN selection with CNN score 0.737. (right) $n - \bar{n}$ cluster passing the BDT pre-selection with BDT score 0.221 and failing the CNN selection with CNN score 0.662.*

C - Simulated Event Display

The event display in Fig 9 represents the final selected cluster using Wire-Cell reconstruction.

Figure 9: *Simulated event display showing one $n - \bar{n}$ simulated event. The x-axis represents z direction (beam direction) and y-axis is the vertical direction. The view in this image is front view (YZ) of the detector. Color represents charge deposition. The signal cluster shown here represents the final selected cluster using Wire-Cell reconstruction.*